Optimal synthesis of a spherical parallel mechanism for medical application

T. Essomba†‡, M. A. Laribi‡, S. Zeghloul‡,* and G. Poisson†

†PRISME Laboratory, University of Orleans, 12, Rue de Blois, 45067 Orleans, France
‡PPRIME Institute, GMSC Department, RoBioSS, CNRS, University of Poitiers, ENSMA, UPR 3346, France
E-mails: terence.essomba@univ-orleans.fr, med.amine.laribi@univ-poitiers.fr, gerard.poisson@univ-orleans.fr

SUMMARY
This paper introduces the design and the optimization of a probe holder robot for tele-echography applications. To define its kinematic architecture, an approach based on motion capture of an expert's gestures during ultrasound examinations was proposed. The medical gestures analyzed consisted of ultrasound probe movements and were used to characterize the kinematic specifications of the proposed manipulator. The selected architecture was a Spherical Parallel Mechanism (SPM) with 3 degrees of freedom (DoF) and its optimal synthesis was performed using real-coded Genetic Algorithms (GA). The optimization criteria and constraints were established thanks to the collaboration of medical experts and were successively formulated and solved using mono-objective and multi-objective functions.

KEYWORDS: Design; Parallel manipulators; Optimal synthesis; Optimization; Medical robot.

1. Introduction

Ultrasonography is a non-invasive technique that allows a medical expert to examine the internal organs of a patient without any side effects. This technique is widely used for many medical examinations. It is cheap, fast, and technically easy to perform and the diagnostic is immediate. However, the execution of this "expert-dependent" technique is compromised in cases of medical expert unavailability, geographical inaccessibility, or inability of displacement. To cope with these problems, robotized tele-echography seemed to be a promising alternative. This technology was created in the 1990s and allows a medical expert to examine patients remotely. More precisely, this expert, located at the "expert premises," uses a control device to operate the tele-echography robot which holds the ultrasound probe acting on the patient at the "patient premises." The expert receives the ultrasound imaging at the "expert premises." Both premises can communicate using satellite, telephone, or internet.

The first robotic system, MIDSTEP, appeared in 1996.[1] The only objective was to validate the concept of ultrasound-guided remote telesurgery using anthropomorphic robots for this system. Since then, other medical robots have appeared with diverse kinematic architectures like Salcudean's pantograph,[2] RUDS,[3] TER,[4] or WTA-2R.[5] Their suitability for specific clinical tasks was much improved. In the present paper, we focus on portable robotic devices. The first portable robot dedicated to tele-echography was created in 1998 by the Vision & Robotics Laboratory. SYRTECH[6] was designed for heart examination. Its main objective was to validate the concept of very long range tele-echography. It was successfully used during an expedition to Nepal: the medical expert in Bourges (France) was able to examine a patient located in Katmandu (Nepal). The success of SYRTECH

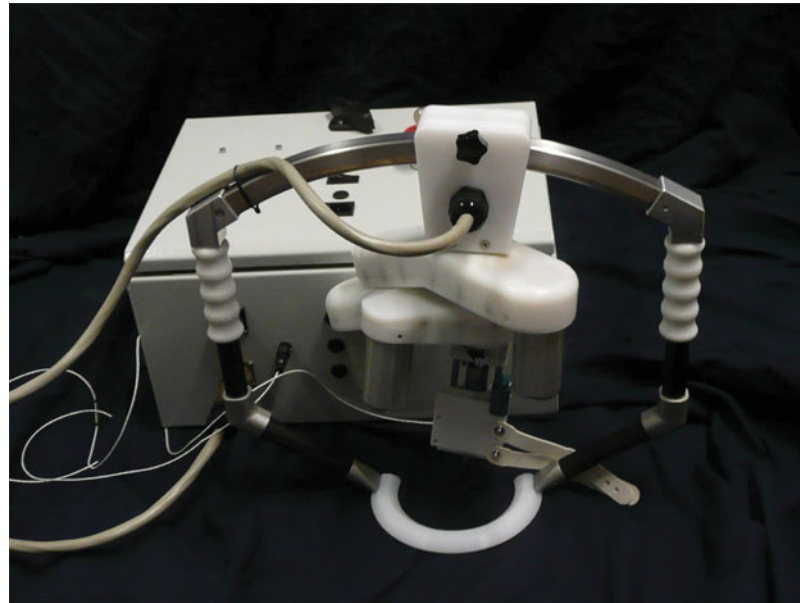* Corresponding author. E-mail: said.zeghloul@univ-poitiers.fr

Fig. 1. Picture of Prosit-1.

resulted in the funding by the European Spatial Agency (ESA) in 2001, of the TERESA project (Tele-Echography Robotized ESA),[7] in order to equip orbital stations. The OTELO-1 and OTELO-2 prototypes (mObile Tele-Echography using an ultra-Light rObot)[8] were developed under a European project in 2003 and 2004 respectively. The objective was to increase the mobility and workspace provided by TERESA. The most advanced tele-echography robot, developed by Vision & Robotics Laboratory named ESTELE, was commercialized by Robosoft in 2006.[9] The system validation was done under the MARTE III project in 2008. The medical expert located in Bourges successfully examined a patient on a boat sailing in the Mediterranean Sea. The newest portable device, FASTele,[10] was designed for the examination of injured patients in a non-clinical environment.

The main objective of the French Agence Nationale de Recherche (ANR) project named PROSIT (Plateforme RObotique d'un Système Intéractif pour la Télé-échographie) was to design an innovative and interactive tele-echography robot.[11] Several scientific, medical, and industrial partners were involved in this project: PRISME Laboratory,[12] INRIA of Rennes,[13] LIRMM Laboratory,[14] PPRIME institute,[15] University Hospital Center of Tours,[16] and Robosoft (French robotic company). The first prototype of the Prosit-1 has been manufactured (Fig. 1).

The current mechanism of commercially available models suffers from the existence of singularities typically located at the center of the workspace; in addition, the rigidity is poor. This constitutes the main disadvantage of tele-echography robots.

One of the objectives of this work was to address these problems by proposing a new mechanism with better performance without increasing the size. In addition, the proposed robot must be more accurate than the previous ones.

Section II of this paper presents the experiments carried out for expert gesture analysis. In Section III, a new kinematic of the future tele-echography robot prototype is detailed. The different formulations of the optimization methods are proposed in Section IV. The last section is dedicated to the conclusions and additional perspectives concerning this work.

2. Expert Gesture Analysis

A set of experiments was carried out in order to analyze the expert's motions that need to be reproducible using the robot. These were performed in a medical environment by recording the motions of medical experts performing ultrasound examinations at the University Hospital Center in Tours city.
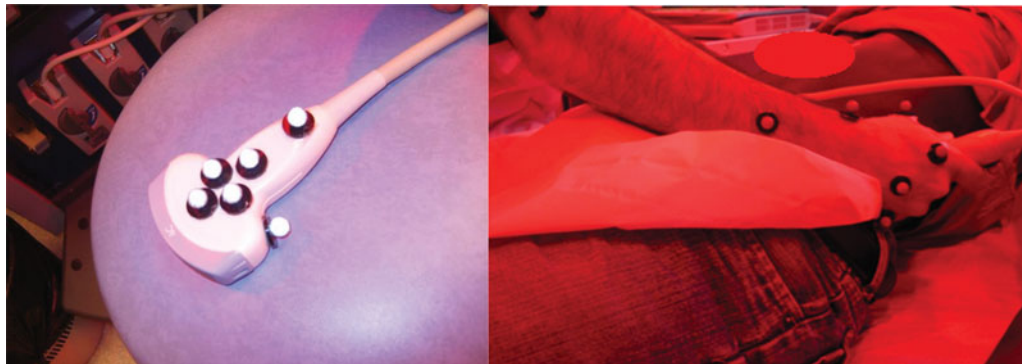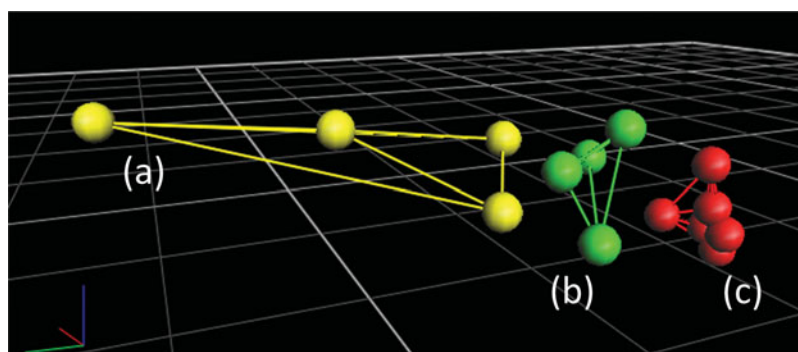
Fig. 2. Picture of reflective markers.

Fig. 3. Reconstruction of several detected markers into segments. Expert's arm (a); expert's hand (b); and ultrasound probe (c).

Expert gesture analysis was performed using the motion capture system Vicon Nexus. Markers were placed on the ultrasound probe as well as on the expert's arm and hand (Fig. 2) in order to record the expert's motions during the examination of patients.[17]

Fourteen patients were examined by four medical experts, which allowed us to record 25 examinations. Nexus software was used to process those records (Fig. 3).

The 3-D coordinates of the markers were used to compute the ultrasound probe orientation. The reference frame of the ultrasound probe was computed using the coordinates of markers placed on it. The unit vectors of this reference were used to establish the rotation matrix which characterizes the probe orientation with respect to the terrestrial frame (see Fig. 4).

The orientation of this frame was computed to determine the Euler angles (ψ, θ, φ) of the probe during the examination using a method presented in Annex A. The results of these measures allowed the characterization of the robot workspace swept by the probe during examinations. For all the examined organs, the orientation workspace was computed. Several organs were selected by medical experts as they were explored systematically during examination routines: the gallbladder, portal vein, pancreas, and kidney. In Fig. 5, the vector $\mathbf{Z}_S$ was associated with the probe's longitudinal direction and was projected on a plane parallel to the skin to evaluate the swept workspace. The extremity trace of this projected vector was plotted in Fig. 5(a) and (b), while the vector origin was the center of the circles. Figures 5 shows the limits of angle θ. We can observe that a value of $45°$ for the θ angle was sufficient for all examinations.

This means that the motions of the probe are within a cone with a maximum apex angle equal to $45°$. However, for most situations, a tilt angle of $35°$ was sufficient according to the medical experts. The results from the expert gesture analysis as well as expert advice were used to establish the specifications of the future tele-echography system. The evolution of the self-rotation angle, φ, during the exploration of several organs, was presented in Fig. 5(c). It was observed through experiments that the examination process requires a self-rotation amplitude of $[-30°; 30°]$ as shown in Fig. 5.
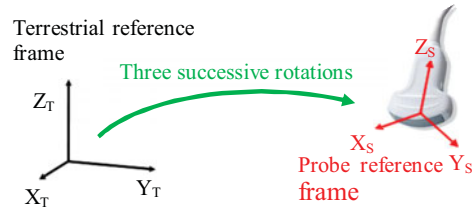
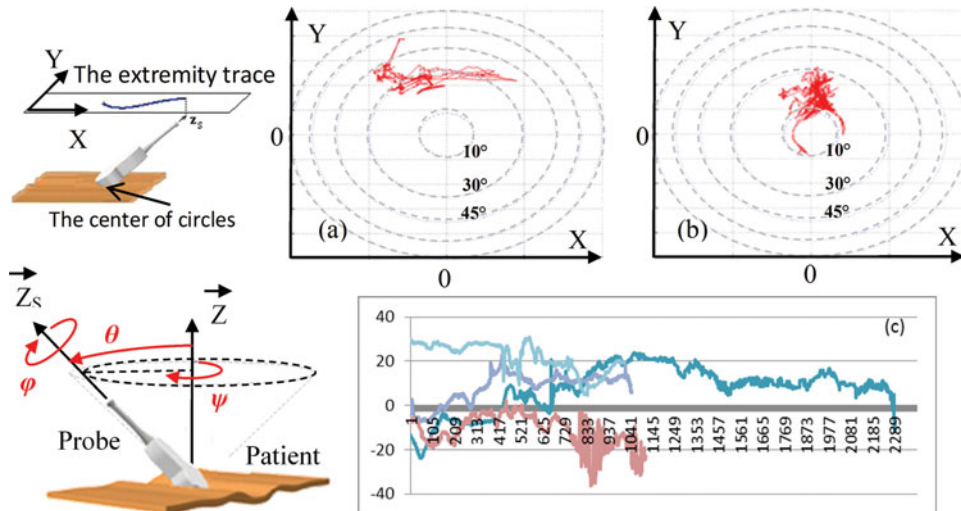Fig. 4. Terrestrial and ultrasound probe reference frames.

Fig. 5. Orientation workspace of the ultrasound probe during the gallbladder (a) and the pancreas (b) exploration. Evolution of angle φ during the exploration of several organs (c).

3. A New Mechanical Architecture for the Tele-Echography Robot

3.1. The spherical parallel mechanism manipulator

The portable robotic manipulator has to conform to several specifications. An important one was to propose an alternative solution to the serial architectures typically developed by the PRISME laboratory in order to increase the kinematic performance. This section introduces the selected architecture which is called Spherical Parallel Mechanism (SPM). The most famous example of such a robot is the Agile Eye of the University of Laval.[18] Another one was developed by the PPRIME Institute for application in mini-invasive surgery (see Fig. 6).[24]

The characteristics of a SPM meet the requirements of tele-echography and avoid the drawbacks found in the previous serial robots. The parallel architecture provides high rigidity, high accuracy, and low inertia in the moving parts.

The SPM is composed of a fixed base and a mobile platform connected by three RRR serial arms. The first revolute joint of each arm is actuated. This parallel structure is able to move its end effector with 3 rotational degrees of freedom (DoF) around a fixed point called the Remote Center of Motion (RCM), as illustrated in Fig. 7. This particular point is located on the contact point between the probe and the patient's skin and must be outside the structure. This is a restrictive constraint and the main difference between the Agile Eye and the proposed robot in this work.

Before studying the kinematic structure, the design parameters that describe the dimensions of the 3-RRR SPM structure must be defined. Each arm of the SPM is composed of two segments whose size can be described by an angular parameter. The dimensions of an arm k are given by angles α_k and β_k. The first revolute joint corresponds to the actuator joint coordinate described by θ_{1k}. The platform size is given by angle γ. The base is composed of a rigid support which orients the first revolute of each arm with angle ξ.

In a previous study, Laribi *et al.*[20] performed an optimization method for the prescribed workspace applied to a 3-RRR SPM. They proved that the symmetric SPM is well adapted for use in
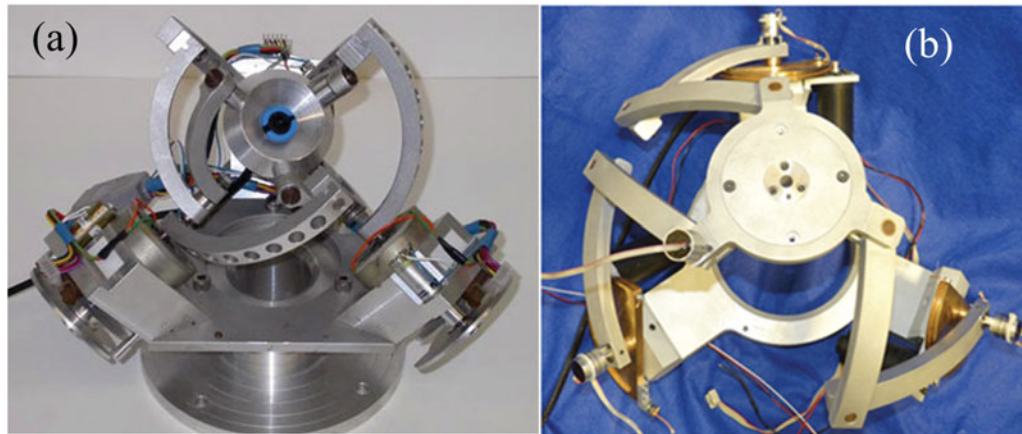
Fig. 6. Picture of the Agile Eye[18] (a) and the PPRIME SPM[19] (b).
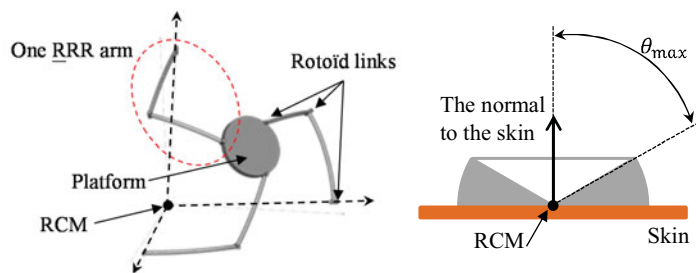
Fig. 7. Kinematic scheme of a SPM.
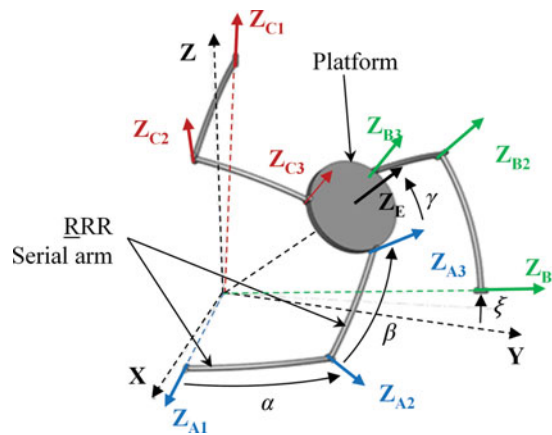
Fig. 8. The design parameters of the SPM.

tele-echography applications. In order to simplify the kinematic model, we focused on a structure with three identical arms. Thereby, the 3-$\underline{R}$RR SPM can be described by the following design vector:

$$\mathbf{D} = \begin{bmatrix} \xi & \alpha & \beta & \gamma \end{bmatrix}^{T}. \tag{1}$$

Fig. 8 shows the design parameters of the SPM.

The inverse kinematic established for each arm k, $k \in \{A, B, C\}$, of the structure is defined as follows:

$$\mathbf{Z}_{2k}.\mathbf{Z}_{3k} = \cos \beta, \tag{2}$$

with

$$\mathbf{Z}_{2A} = \mathbf{R}_X(\theta_{A1}) \cdot \mathbf{R}_Z(\alpha) \cdot \mathbf{Z}_{1A}, \tag{3}$$

$$\mathbf{Z}_{2B} = \mathbf{R}_Y(\theta_{B1}) \cdot \mathbf{R}_X(\alpha) \cdot \mathbf{Z}_{1B}, \tag{4}$$

$$\mathbf{Z}_{2C} = \mathbf{R}_Z(\theta_{C1}) \cdot \mathbf{R}_Y(\alpha) \cdot \mathbf{Z}_{1C} \tag{5}$$

and

$$\mathbf{Z}_{3A} = \mathbf{M}_E \cdot \mathbf{R}_Y(\gamma) \cdot \mathbf{Z} \tag{6}$$

$$\mathbf{Z}_{3B} = \mathbf{M}_E \cdot \mathbf{R}_Z\left(\frac{2\pi}{3}\right) \cdot \mathbf{R}_Y(\gamma) \cdot \mathbf{Z}, \tag{7}$$

$$\mathbf{Z}_{3C} = \mathbf{M}_E \cdot \mathbf{R}_Z\left(-\frac{2\pi}{3}\right) \cdot \mathbf{R}_Y(\gamma) \cdot \mathbf{Z}. \tag{8}$$

$\mathbf{R}_X$, $\mathbf{R}_Y$, and $\mathbf{R}_Z$ represent the rotation matrices around the $\mathbf{X}$, $\mathbf{Y}$, and $\mathbf{Z}$ axes and the Euler matrix $\mathbf{M}_E$. Their literal expressions are detailed in Annex B.

The equations obtained from Eq. (2) can be decoupled to yield the following three scalar equations involving variables θ_{1k}, ψ, θ, and φ:

$$\begin{cases} L_A\cos(\theta_{1A}) + M_A\sin(\theta_{1A}) = N_A \\ L_B\cos(\theta_{1B}) + M_B\sin(\theta_{1B}) = N_B \\ L_C\cos(\theta_{1C}) + M_C\sin(\theta_{1C}) = N_C \end{cases}. \tag{9}$$

Eq. (9) are resolved to obtain the expression of the actuator coordinate:

$$\theta_{1k} = \cos^{-1}\left(\frac{N_k}{\sqrt{L_k^2 + M_k^2}}\right) + \alpha, \tag{10}$$

with $\alpha = \text{atan2}(M_k, L_k)$.

L_k, M_k, and N_k are constant functions of the geometric parameters and ψ, θ, and φ, which are the end effector Euler angles.

3.2. Kinematic analysis

The velocity model can be obtained by differentiating Eq. (2) with respect to time. The obtained equation can be written as:

$$\mathbf{Z}_{2k} \, \mathbf{Z}_{3k} + \mathbf{Z}_{2k} \, \mathbf{Z}_{3k} = 0, \tag{11}$$

with

$$\mathbf{Z}_{2k} = \theta_{1k} \, \mathbf{Z}_{1k} \times \mathbf{Z}_{2k} \tag{12}$$

and

$$\mathbf{Z}_{3k} = \omega \times \mathbf{Z}_{3k}. \tag{13}$$

ω is the angular velocity vector of the end effector. We obtain:

$$\theta_{1k}\mathbf{Z}_{1k} \times \mathbf{Z}_{2k} \cdot \mathbf{Z}_{3k} = -\mathbf{Z}_{2k} \cdot \omega \times \mathbf{Z}_{3k}, \tag{14}$$

$$\mathbf{Z}_{1k} \times \mathbf{Z}_{2k} \cdot \mathbf{Z}_{3k}\theta_{1k} = \mathbf{Z}_{2k} \times \mathbf{Z}_{3k} \cdot \omega. \tag{15}$$

For the whole manipulator, we have

$$\mathbf{B}q = \mathbf{A}\omega, \tag{16}$$

where **B** is a 3×3 diagonal matrix:

$$\mathbf{B} = \begin{bmatrix} \mathbf{Z}_{1B} \times \mathbf{Z}_{2B} \cdot \mathbf{Z}_{3B} & 0 & 0 \\ 0 & \mathbf{Z}_{1B} \times \mathbf{Z}_{2B} \cdot \mathbf{Z}_{3B} & 0 \\ 0 & 0 & \mathbf{Z}_{1C} \times \mathbf{Z}_{2C} \cdot \mathbf{Z}_{3C} \end{bmatrix}, \quad (17)$$

and

$$\mathbf{q} = [\theta_{1A} \; \theta_{1B} \; \theta_{1C}]^{T}, \quad (18)$$

$$\mathbf{A} = \begin{bmatrix} (\mathbf{Z}_{2A} \times \mathbf{Z}_{3A})^{T} \\ (\mathbf{Z}_{2B} \times \mathbf{Z}_{3B})^{T} \\ (\mathbf{Z}_{2C} \times \mathbf{Z}_{3C})^{T} \end{bmatrix}, \quad (19)$$

$$\omega = \begin{bmatrix} \theta \cos(\psi) + \phi \sin(\theta) \sin(\psi) \\ \theta \sin(\psi) - \phi \sin(\theta) \cos(\psi) \\ \psi + \phi \cos(\theta) \end{bmatrix}. \quad (20)$$

The problem of non-homogeneity in the Jacobean matrix is not encountered in the present case since the SPM only has orientation DoF. Therefore, the condition number can be a reliable measure of dexterity. The model can be written as

$$\omega = \mathbf{J}\mathbf{q} = \mathbf{A}^{-1}\mathbf{B}\,\mathbf{q}. \quad (21)$$

The solution of the inverse model and the Jacobian matrix are used to study the criteria and constraints to be integrated during the optimization process.

4. Optimization Process of the Spherical Parallel Mechanism

The 3-RRR SPM has been studied in several works. The design of the SPM was considered from the kinematic viewpoint by Gosselin *et al.*[27,28] Three criteria are considered (symmetry, workspace maximization, and isotropy). Takeda *et al.*[29] proposed a new mechanism design method using a transmission index calculated from only geometrical conditions. A parallel manipulator with a large workspace in which motion transmissibility is excellent and interferences among links do not occur was proposed. Other evaluation criteria including a stiffness aspect were proposed by Liu *et al.*[30] to select the link lengths of 3-DoF SPM and to analyze the operational performance.

In this work, several criteria were selected in agreement with medical experts and were used in the optimization process. These criteria allow for the identification of the most suitable 3-RRR SPM.

The first step of the process was to establish an efficient interpretation of these criteria to obtain quantitative criteria. Three aspects were taken into consideration. The manipulator must generate the workspace identified by expert gesture analysis and presented in Section 2. The robot must have high accuracy. Since the robot is portable and maintained by a medical assistant on the patient during the ultrasound exam, it needs to be light and compact.

4.1. Constraints and criteria

The design optimization problem for the 3-DoF SPM considers the kinematic performance, the specified workspace, and the compactness.

4.1.1. Workspace. The workspace was not considered as a criterion to be optimized but as a constraint in the optimization process. A structure which is unable to respect this constraint is rejected. The expert gesture analysis indicated that the workspace was a cone with apex angle of $35°$. This means that the manipulator must be able to tilt the ultrasound probe up to $35°$. If the structure is able to reach a point of the workspace, then the inverse kinematic expression of each arm has a solution for

the considered orientation of the platform. The existence condition is the following (Eq. (10)):

$$\left| \frac{N_k}{\sqrt{M_k^2 + L_k^2}} \right| \leq 1. \tag{22}$$

The orientation of the platform is given by the Euler angles (ψ, θ, φ). The three operational variables are defined by three bounding intervals as follows: $\psi \in [0, 2\pi]$, $\theta \in [0, \theta_{WS}]$, and $\varphi \in [-\varphi_{WS}, \varphi_{WS}]$. All of these variables are considered during the synthesis of the full parallel manipulator.

Condition (22) is then used to define the orientation power function $S_k(\psi, \theta, \varphi)$, which indicates if arm k is able to reach the given orientation or not. The orientation power function is defined as follows:

$$S_k (\psi, \theta, \varphi) = L_k^2 + M_k^2 - N_k^2, \tag{23}$$

with $k = $ A, B, or C.

Therefore, one can state that for a given orientation vector $\Phi = [\psi_D, \theta_D, \varphi_D]^T$.

- If Φ is reachable by all the arms then $S_k(\psi_D, \theta_D, \varphi_D) < 0$ for $k = $ A, B, and C.
- If Φ is on the boundary of the workspace then $S_k(\psi_D, \theta_D, \varphi_D) \leq 0$ for $(k = $ A, B, and C) and $S_k(\psi_D, \theta_D, \varphi_D) = 0$ for $(k = $ A) or $(k = $ B) or $(k = $ C).
- If Φ is unreachable by arm K then $S_k(\psi_D, \theta_D, \varphi_D) > 0$ for $k = $ A, B, or C.

The power function is then integrated into a formulation, it indicates if a structure respects the workspace constraints.

For a given structure described by the design vector $\mathbf{D} = [\xi \quad \alpha \quad \beta \quad \gamma]^T$, the workspace value can be written as:

$$W_D = \sum_{\varphi=-\varphi_{WS}}^{\varphi_{WS}} \sum_{\psi=0}^{n} \sum_{\theta=0}^{m} P_W (\psi, \theta, \phi), \tag{24}$$

with $n = 2\pi/\Delta\psi$, $m = \theta_{ws}/\Delta\theta$, and $\theta_{WS} = 35°$ maximum angle. $P_W(\psi, \theta, \varphi)$ is an incremental function with respect to S_k.

$$P_W (\psi, \theta, \varphi) = \begin{cases} 1 & si\, S_{A,B,C} (\psi, \theta, \varphi) > 0 \\ 0 & si\, S_{A,B,C} (\psi, \theta, \varphi) \leq 0 \end{cases}. \tag{25}$$

W_D gives the number of unreachable points in the necessary workspace. A zero value for W_D means the whole workspace is reachable.

4.1.2. Dexterity. In the literature, several methods and indices can be found in: Yoshikawa,[21] Angeles,[22] and Gosselin[23] to compute different dexterity indices. To compute the kinematic performance of a structure, we chose the global dexterity method proposed by Gosselin as it characterizes the isotropy of the robot.

A commonly used criterion to evaluate this kinematic performance is the global conditioning index η_D^G, which describes the isotropy of the kinematic performance. The index, for a given structure described by the design vector $\mathbf{D}$, is defined over a workspace Ω as :

$$\eta_D^G = \frac{\int_\Omega \eta_D^L dw}{\int_\Omega dw}, \tag{26}$$

where η_D^L is the local dexterity and $\kappa(\mathbf{J})$ is the condition number of the kinematic Jacobian matrix (21) defined by
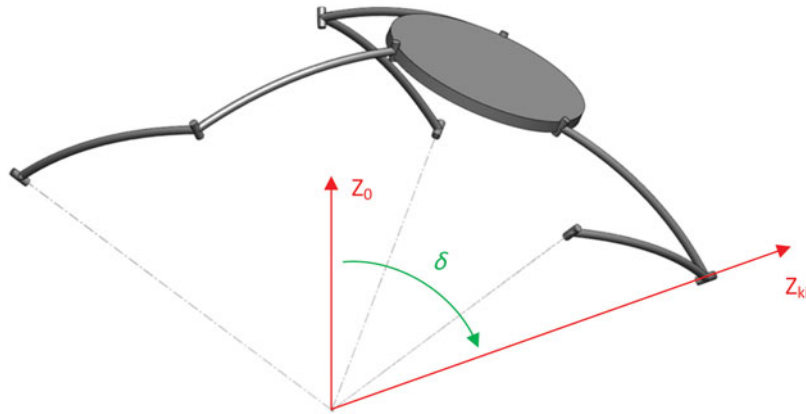
$$\eta_D^L = \frac{1}{\kappa (\mathbf{J})}. \tag{27}$$

Fig. 9. Illustration of the most inclined axis.

In practice, the global conditioning index η_{D}^{G} of a robotic manipulator is calculated through a discrete approach as

$$\eta_{\mathrm{D}}^{G} = \frac{\sum_{\varphi=-\varphi_{ws}}^{\varphi_{ws}} \sum_{\psi=0}^{n} \sum_{\theta=0}^{m} \frac{1}{\kappa(\mathbf{J})} \Delta\psi \, \Delta\theta \, \Delta\varphi}{\sum_{\varphi=-\varphi_{ws}}^{\varphi_{ws}} \sum_{\psi=0}^{n} \sum_{\theta=0}^{m} \Delta\psi \, \Delta\theta \, \Delta\varphi}. \tag{28}$$

Both indices vary between 0 (poor) and 1 (optimal). In the next section, the local distribution of the dexterity over the workspace using local dexterity was studied.

4.1.3. Compactness. The compactness performance indicates the volume occupied by the structure in a given configuration. Here, its value depends on the angle of the most inclined robot axis, δ. If $\mathbf{Z}_0$ is the central vector of the structure (see Fig. 9), one can compute this angle for a given configuration as follows:

$$\delta = \max_{k,i} \left(\mathrm{acos} \left(\mathbf{Z}_0 . \mathbf{Z}_{ki} \right) \right), \tag{29}$$

with $k = $ A, B, or C and $i = 1, 2,$ or 3.

This angle is then integrated in the definition of the local compactness λ_{D}^{L} (30). This index represents the ratio between angle δ of the most inclined axis and the $\theta_{\max}$ maximum safety angle that we have set to $85°$.

$$\lambda_{\mathrm{D}}^{L} = 1 - (\delta / \theta_{\max}). \tag{30}$$

As for the dexterity, it is possible to study this index in a local position but also with a global point of view by integration of the local compactness λ_{D}^{L} over the workspace. The index, for a given structure described by the design vector $\mathbf{D}$, is defined over a workspace Ω as:

$$\lambda_{\mathrm{D}}^{G} = \frac{\int_{\Omega} \lambda_{\mathrm{D}}^{L} dw}{\int_{\Omega} dw}. \tag{31}$$

In practice the integral is calculated through a discrete approach as

$$\lambda_{\mathrm{D}}^{G} = \frac{\sum_{\varphi=-\varphi_{ws}}^{\varphi_{ws}} \sum_{\psi=0}^{n} \sum_{\theta=0}^{m} \lambda_{\mathrm{D}}^{L} \Delta\psi \, \Delta\theta \, \Delta\varphi}{\sum_{\varphi=-\varphi_{ws}}^{\varphi_{ws}} \sum_{\psi=0}^{n} \sum_{\theta=0}^{m} \Delta\psi \, \Delta\theta \, \Delta\varphi}. \tag{32}$$

Both indexes vary from 0 (poor compactness) to 1 (good compactness).

4.2. Formulation of the problem

The aim of this section is to solve the multidimensional, non-linear optimization problem of selecting the geometric design variables for the SPM. The SPM must reach a specified workspace with a high dexterity and compactness.

The proposed approach is based on three different formulations. The first one is a multi-objective maximization of two objective functions (dexterity and compactness) using a Genetic Algorithms (GA) method. The second approach performs an optimization through aggregation of two functions. The third formulation considers the compactness as an additional constraint and the dexterity as an objective function.

Before developing these formulations, the optimization process via a GA method will be specified briefly.

4.2.1. Genetic algorithms method. Genetic Algorithms are heuristic search algorithms based on the mechanisms of natural selection and natural genetics initially proposed by Holland.[25] They have been used in a variety of engineering fields such as in machine design. A real-coded GA[26] is used here to solve the optimization problem.

In the present application, each individual is a design vector. $\mathbf{D} = [\xi \quad \alpha \quad \beta \quad \gamma]$. It corresponds to a 3-RRR SPM and their characteristics are design parameters. A population of 50 individuals is manipulated through 100 generations. Crossover and mutation rates are respectively set to 10% and 5%.

The algorithm is allowed to select design parameter values in the following interval:

$$\xi \in [-20; 20] \, \alpha \in [20; 75] \, \beta \in [20; 75] \, \gamma \in [15; 35] . \tag{33}$$

In the last generation, the individual that generates the best fitness value (objective function value) is selected as the optimal SPM. The main objective was to identify the design vector corresponding to the structure that generates the necessary workspace and the best combination of dexterity and compactness. A penalty function was used to handle the constraints and to ensure that the fitness of any feasible solution is better than the non-feasible ones.

4.2.2. First approach. This can be stated as

$$\text{Maximize} : (f_d(\mathbf{D}), f_c(\mathbf{D})), \tag{34}$$

subject to: $W_\mathbf{D} = 0$, see Eq. (24).

$$x_i \in [x_{i\min}; x_{i\max}], \qquad x_i \in \mathbf{D}; \; \mathbf{D} = \begin{bmatrix} \xi & \alpha & \beta & \gamma \end{bmatrix}^T ,$$

where $f_d(\mathbf{D}) = \eta_\mathrm{D}^G$ and $f_c(\mathbf{D}) = \lambda_\mathrm{D}^G$.

The vector $\mathbf{D}$ contains the independent design variables, x_i, called individual in the GA technique. The range of each design variable is given by $x_{i\min}$ and $x_{i\max}$.

The objective function, in this formulation, includes two criteria (Eq. (30)). All potential solutions that optimize $f_d(\mathbf{D})$ and $f_c(\mathbf{D})$ are located in a Pareto front (Fig. 10). Their positions in the Pareto front correspond to a solution with a low global compactness and high global dexterity. Indeed, their values go from 0.359 to 0.461 for dexterity and from 0.021 to 0.053 for compactness. For these ranges, there is no method to increase the value of one criterion without compromising the other. For instance, one can decrease the global compactness, however, this necessarily implies the presence of negative local compactness which indicates a constraint violation and consequently the individual is rejected.

In this study, both criteria are set to be of equal weight for the optimization. As a result, the compactness is hardly modified compared to the dexterity. For this reason, a mono-objective study is proposed to change the weight of each criterion and study the influence on the optimization results.

4.2.3. Second approach. The second approach is an aggregation approach goal, whose purpose is to study the evolution of the two optimization criteria which are contradictory. This can be stated as:
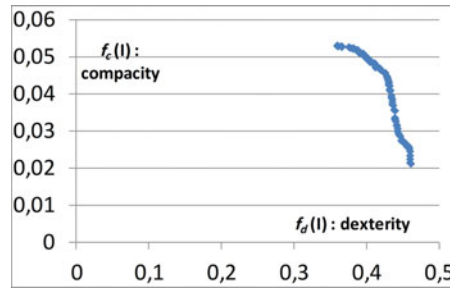
$$\text{Maximize} \, (f_\varepsilon(\mathbf{D})), \tag{35}$$

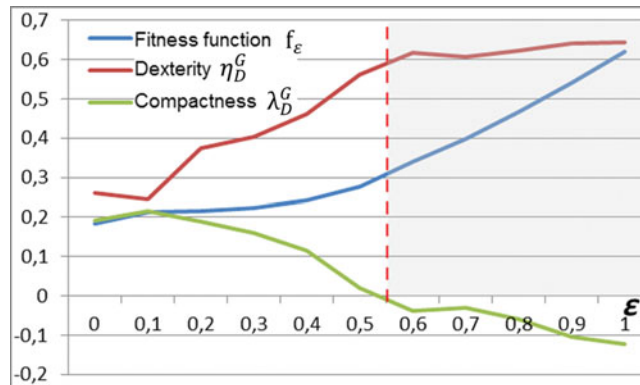Fig. 10. Pareto front of the optimal generation of 3-RRR SPM.

Fig. 11. Evolution of the fitness function versus ε.

subject to: $W_{\mathbf{D}} = 0$.

$$x_i \in [x_{i\min}; x_{i\max}] \qquad x_i \in \mathbf{D}; \; \mathbf{D} = \begin{bmatrix} \xi & \alpha & \beta & \gamma \end{bmatrix}^T ,$$

where $f_\varepsilon(\mathbf{D}) = \eta_D^G \varepsilon + \lambda_D^G (1 - \varepsilon)$ and $\varepsilon \in [0, 1]$.

The weighting factor ε is used to set each criterion's weight. Priority is given to the global dexterity when ε tends towards 1 and to global compactness when it tends towards 0.

An optimization process is performed with a fitness function $f_\varepsilon(\mathbf{D})$. The optimization, as stated in Eq. (35), was solved for each value of the ε weighting factor. The evolution of the fitness function versus ε is shown in Fig. 11, the corresponding dexterity and compactness are also represented.

The value of the fitness function increases with ε. It means that for this type of structure, it is easier to generate a good dexterity than a good compactness. In fact, the global dexterity is still higher than 0.25 even if ε is close to zero whereas the global compactness becomes negative when ε is higher than 0.5.

The above optimization methods have highlighted the difficulty in maintaining both the dexterity and the compactness at a high level. Giving priority to dexterity leads to a structure having good dexterity but with large dimensions which causes external collisions (between the robot and the patient). In this case, the approach leads to solution very close to the Agile Eye which results from an optimization process based on the dexterity criterion.[18] When the priority is given to compactness, the SPM obtained is free of external collisions but it generates poor dexterity. It is obvious that compactness is not easy to optimize without altering the dexterity. This is why it was proposed to consider the compactness as a constraint in the third formulation described in the next section.

4.2.4. Third approach. Consequently, compactness was now a constraint that guaranteed that the considered structure is free of any external collisions. A negative local compactness indicated that the angle δ exceeds the maximum safety angle (Eq. (30)). The local compactness must be positive
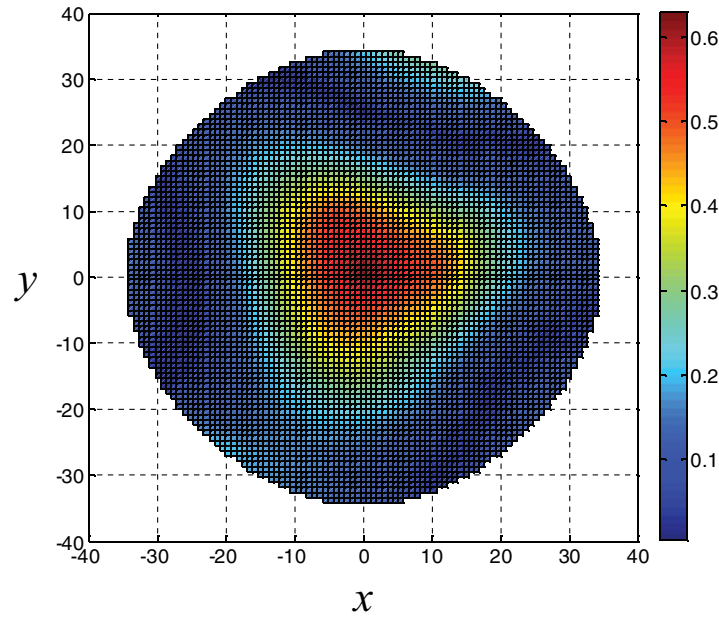
Fig. 12. Distribution of the SPM dexterity in the Cartesian workspace.

for all orientations of the end effector to verify the absence of external collisions:

$$C_D = \sum_{\varphi=-\varphi_{ws}}^{\varphi_{ws}} \sum_{\psi=0}^{n} \sum_{\theta=0}^{m} P_C(\psi, \theta, \varphi), \tag{36}$$

where $n = 2\pi/\Delta\psi$ and $m = \theta_{ws}/\Delta\theta$,
where the maximum angle $\theta_{WS} = 35°$,
where $P_C(\psi, \theta, \varphi)$ function is defined by

$$\begin{cases} P_C(\psi, \theta, \varphi) = 0 \, si \, \lambda_D(\psi, \theta, \varphi) > 0 \\ P_C(\psi, \theta, \varphi) = 1 \, si \, \lambda_D(\psi, \theta, \varphi) \le 0 \end{cases}. \tag{37}$$

C_D is the number of orientations of the end effector that generate an external collision. When C_D is zero, the entire workspace is free of external collision.

This optimization process identifies the most dexterous 3-RRR SPM that generates the necessary workspace. The obtained solution is free of any external collision since it respects the constraints. The problem formulation can be written as follows:

$$\text{Maximize}\left(F(\mathbf{D}) = \eta_D^G\right), \tag{38}$$

subject to: $\begin{array}{l} W_\mathbf{D} = 0 \\ C_\mathbf{D} = 0 \end{array}$, see Eqs. (24) and (36).

$$x_i \in \mathbf{D} \qquad x_i \in [x_{i\min}; \ x_{i\max}].$$

The GA was used with these new parameters with the resulting design vector as the following: $\mathbf{D}_{opt} = [2.94°, 33.15°, 32.54°, 25.86°]$, which lead to a structure with $0 \le \psi \le 2\pi$, $0 \le \theta \le \theta_{WS}$, and $-\varphi_{WS} \le \varphi \le \varphi_{WS}$.

This structure has a global dexterity of 0.284 over its workspace which is 2.5 times higher than Prosit-1 (Fig. 1). The maximum local dexterity of 0.637 in the center of its workspace is four times higher than Prosit-1. The minimal value of the local dexterity over the whole workspace remained at about 62% of the maximum value. This minimal value was reached when one RRR arm was completely folded. The dexterity distribution of the optimal SPM is illustrated in Fig. 12.
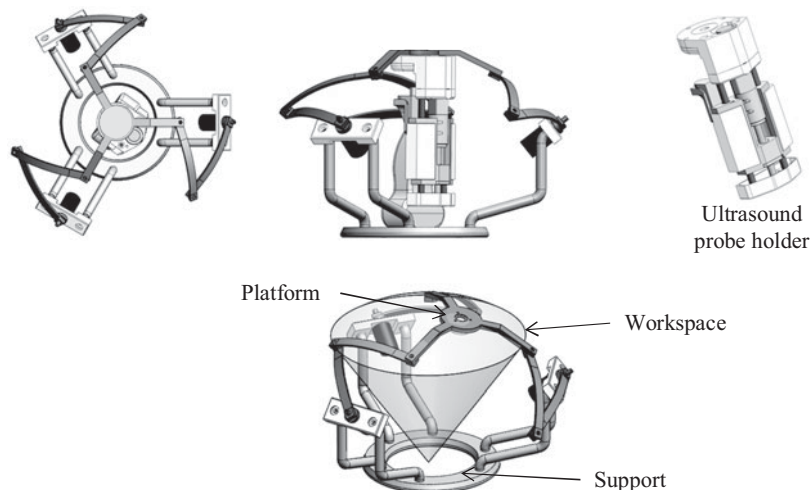
Fig. 13. Computer-aided design illustration of the optimization SPM.

Figure 13 shows a CAD illustration of the optimized structure including the workspace. It is represented as a cone with a 35° apex angle.

5. Conclusion

The objective of this approach was to propose an optimized mechanical architecture for tele-operated ultrasound examinations. Several specifications were established with the collaboration of medical experts. An expert gesture analysis was carried out to provide numerical evidence for these specifications. They were integrated into the design process to optimize a new architecture for this type of application. The global dexterity, the global compactness, and the workspace were selected as kinematic performance criteria and constraints for the SPM architecture.

Three approaches based on optimization processes have been proposed with different objective functions and solved using a real coded GA.

The obtained structure increases the kinematic performance when compared to previously manufactured robots of our laboratory.

References
1. D. de Cunha, P. Gravez, C. Leroy, E. Maillard, J. Jouan, P. Varley, M. Jones, M. Halliwell, D. Hawkes, P. N. T. Wells and L. Angelini, "The MIDSTEP System for Ultrasound Guided Remote Telesurgery," *Proceedings of 20th International Conference of the IEEE Engineering in Medicine and Biology Society*, Hong Kong (Oct. 29-Nov. 1, 1998) pp. 1266–1269.
2. S. E. Salcudean, W. H. Zhu, P. Abolmaesumi, S. Bachmann and P. D. Lawrence, "A robot system for medical ultrasound," Proceedings of *ISRR'99*, Snowbird, USA (Oct. 9–12, 1999) pp.152–159.
3. M. Mitsuishi, S. Warisawa, T. Tsuda, T. Higuchi, N. Koizumi, H. Hashizume and K. Fujiwara, "Remote Ultrasound Diagnostic System," Proceedings of *IEEE ICRA*, vol. 2, South Korea (May 21–26, 2001) pp. 1567–1573.

4. A. Vilchis, J. Troccaz, P. Cinquin, F. Courrèges, G. Poisson and B. Tondu, "Robotic Tele-ultrasound System (TER): Slave Robot Control," *Proceedings of IFAC Conference on Telematics Application in Automation and Robotics*, Weingarten, Germany (Jul. 24–26 2001) pp 95–100.

5. R. Nakadate, Y. Matsunaga, J. Solis, A. Takanishi, E. Minagawa, M. Sugawara and K. Niki, "Development of a robot assisted carotid blood flow measurement system," *Mech. Mach. Theory* **46**(8), 1066–1083 (2011).

6. A. Gourdon, P. Poignet, G. Poisson, Y. Parmantier and P. March. "Master–Slave Robotic System for Ultrasound Scanning," *Proceedings Eur. Medical and Biological Engineering Conference*, vol. 2, Vienna (Mar. 1999) pp. 1116–1117.

7. P. Vieyres, G. Poisson, F. Courrèges, O. Mérigeaux and Ph. Arbeille, "The TERESA project: From space research to ground tele-echography," *Int. J. Ind. Robot.*, **30**(1), 77–82 (2003).

8. C. Delgorge, F. Courreges, L. Al Bassit, C. Novales, C. Rosenberger, N. Smith-Guerin, C. Bru, R. Gilabert, M. Vannoni, G. Poisson and P. Vieyres, "A tele operated mobile ultrasound scanner using a light weight robot," *IEEE Trans. Innov. Technol. Biomed.*, **9**(1), 50–58 (Mar. 2005).

9. F. Bruyère, J. Ayoub and P. Arbeille, "Use of a telerobotic arm to perform ultrasound guidance during renal biopsy in transplant recipients: a preliminary study," *J. Endourol.* **20**(2), 231–234 (Feb. 2011).

10. K. Ito, S. Sugano and H. Iwata, "Portable and Attachable Tele-echography Robot System: FASTele," *Conference Proceeding of IEEE Engineering in Medicine and Biology Society*, Buenos Aires (Aug. 31– Sep. 4, 2010) pp. 487–490.

11. G. Charron, N. Morette, T. Essomba, P. Vieyres, J. Canou, P. Fraisse, S. Zeghloul, A. Krupa, P. Arbeille and the Prosit Consortium, "Robotic Platform for an Interactive Tele-echographic System: the PROSIT ANR-2008 Project," *Proceedings of the Hamlyn Symposium on Medical Robotics*, London, UK (May 25, 2010) pp. 1–2.

12. G. A. Triantafyllidisa, N. Thomosa, C. Canerob, P. Vieyres and M. G. Strintzis. "A user interface for mobile robotized tele-echography," *Nucl. Instrum. Methods Phys. Res.*, A **569**, 645–648 (2006).

13. R. Mebarki, A. Krupa and F. Chaumette, "Image moments-based ultrasound visual servoing," *ICRA'08*, Pasadena, CA (May 2008).

14. P. Fraisse, P. Dauchez and F. Pierrot. "Robust force control strategy based on virtual environment," *Adv. Robot. J., Robot. Soc. Jpn.* **21**(3–4), 485–498 (2007).

15. S. Zeghloul and P. Rambeaud, "A fast algorithm for distance calculation between convex objects using the optimization approach," *Robotica J.* **14**, 355–363 (1996).

16. P. Arbeille, A. Capri, J. Ayoub, V. Kieffer and G. Poisson. "Use of a robotic arm to tele-operated abdominal ultrasound," *Am. J. Roentgenol.* **188**, 317–322 (2007).

17. T. Essomba, M. A. Laribi, J. P. Gazeau, S. Zeghloul and G. Poisson, "Contribution to the design of a robotized tele-echography system," *Front. Mech. Eng.* **7**(2), 135–149 (2012).

18. C. Gosselin and J. Hamel, "The Agile Eye: A High-Performance Three-Degree-of-Freedom Camera-Orienting Device," *Proceedings of IEEE International Conference on Robotics and Automation*, San Diego, USA (May 8–13, 1944) pp. 781–786.

19. A. Charker, A. Mlika, M. A. Laribi, L. Romdhane and S. Zeghoul, "Synthesis of a spherical parallel manipulator for a dexterous medical task," *Front. Mech. Eng.* **7**(2), 150–162 (2012).

20. M. A. Laribi, T. Essomba, S. Zeghloul and G. Poisson, "Optimal Synthesis of a New Spherical Parallel Mechanism for Application to Tele-echography Chain," *Proceedings of the 2011 ASME IDETC/CIE*, Washington DC, USA (Aug. 28–31, 2011) pp. 579–587.

21. T. Yoshikawa, "Manipulability of robotic mechanisms," *Int. J. Robot. Res.* **4**(2), 3–9 (1985).

22. J. Angeles, F. Ranjbaran and R. V. Patel, "On the Design of the Kinematic Structure of Seven-axes Redundant Manipulators for Maximum Conditioning," *Proceedings of the IEEE International Conference on Robotics and Automation*, Nice, France (May 12–14, 1992) pp. 494–499.

23. C. Gosselin and J. Angeles, "A global performance index for the kinematic optimisation of robotic manipulators," *ASME J. Mech. Des.* **113**(3), 220–226 (1991).

24. A. Chaker, M.A. Laribi, S. Zeghloul and L. Romdhane, "Design and Optimization of Spherical Parallel Manipulator as a Haptic Medical Device," *Proceedings of the 37th IEEE Annual Conference on Industrial Electronics Society*, Melbourne, Australia (Nov. 7–10, 2011), pp. 80–85.

25. D. E. Goldberg, *Genetic Algorithms in Search, Optimization, and Machine Learning* (Addison-Wesley Publishing, Massachusetts, 1994).

26. M. A. Laribi, A. Mlika, L. Romdhane and S. Zeghloul, "A combined genetic algorithm-fuzzy logic method (GA-FL) in mechanisms synthesis," *Mech. Mach. Theory* **39**(7), 717–735 (2004).

27. C. Gosselin and J. Angeles, "The optimum kinematic design of a spherical three degree of freedom parallel manipulator," *Trans. ASME, J. Mech. Transm. Autom. Des.* **111**, 202–207 (1989).

28. C. Gosselin, E. St-Pierre and M. Gagne, "On the development of the agile eye: mechanical design, control issues and experimentation," *IEEE Robot. Autom. Soc. Mag.* **3**(4), 29–37 (1996).

29. Y. Takeda, H. Funabashi and Y. Sasaki, "Development of a spherical in-parallel actuated mechanism with three degrees of freedom with large working space and high motion transmissibility," *JSME Int. J., C* **39**(3), 541–548 (1996).

30. X.-J. Liu, Z.-L. Jin and F. Gao, "Optimum design of 3-dof spherical parallel manipulators with respect to the conditioning and stiffness indices," *Mech. Mach. Theory* **35**, 1257–1267 (2000).

Annex A

Identification of Euler angles of probe

To establish the rotation matrix $\mathbf{R}_T$, the coordinates of each unit vector $(\mathbf{x}_s, \mathbf{y}_s, \mathbf{z}_s)$ of the related reference frames are simply placed in the matrix the following way:

$$\mathbf{R}_T = \begin{bmatrix} x_X & y_X & z_X \\ x_Y & y_Y & z_Y \\ x_Z & y_Z & z_Z \end{bmatrix}, \tag{39}$$

with $\mathbf{x}_s = \begin{pmatrix} x_X \\ x_Y \\ x_Z \end{pmatrix}$, $\mathbf{y}_s = \begin{pmatrix} y_X \\ y_Y \\ y_Z \end{pmatrix}$ et $\mathbf{z}_s = \begin{pmatrix} z_X \\ z_Y \\ z_Z \end{pmatrix}$.

The terms of the obtained matrix are used to compute the orientation angles of the reference frame. The Euler angles are used to define the orientation, as illustrated in Fig. 14:
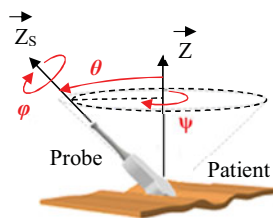

Fig. 14. Illustration of Euler angles.

Euler angle rotation matrix is:

$$R_T = \begin{bmatrix} C\psi C\varphi - S\psi C\theta S\varphi & -C\psi S\varphi - S\psi C\theta C\varphi & S\psi S\theta \\ S\psi C\varphi + C\psi C\theta S\varphi & -S\psi S\varphi + C\psi C\theta C\varphi & -C\psi S\theta \\ S\theta S\varphi & S\theta C\varphi & C\theta \end{bmatrix}, \tag{40}$$

where $C\alpha = \cos\alpha$ and $S\alpha = \sin\alpha$.

The following solution is used:

$$\theta = \mathrm{acos}\, z_Z, \tag{41}$$

$$\psi = \mathrm{atan2}\left(\frac{z_X}{\sin\theta}, \frac{-z_Y}{\sin\theta}\right), \tag{42}$$

$$\varphi = \mathrm{atan2}\left(\frac{x_Z}{\sin\theta}, \frac{y_Z}{\sin\theta}\right). \tag{43}$$

Annex B

Vectors $\mathbf{z}_{2k}$ and $\mathbf{z}_{2k}$ calculations

To solve the SPM inverse kinematic, the literal expressions of axes $\mathbf{Z}_{2k}$ and $\mathbf{Z}_{3k}$ with $k \in \{A, B, C\}$ need to be determined.

Axes Z_{2k} are written with respect of θ_{1k} which are the unknown actuator coordinates. In Eqs. (3) to (5), axes $\mathbf{Z}_{1k}$ are replaced by successive rotation around intermediate axes $\mathbf{X}, \mathbf{Y}$, and $\mathbf{Z}$:

$$\mathbf{Z}_{2A} = \mathbf{R}_X(\theta_{A1}) \cdot \mathbf{R}_Z(\alpha) \cdot \mathbf{R}_X\left(\pi/4\right) \cdot \mathbf{R}_Z(\omega) \cdot \mathbf{X}, \tag{44}$$

$$\mathbf{Z}_{2B} = \mathbf{R}_Y(\theta_{B1}) \cdot \mathbf{R}_X(\alpha) \cdot \mathbf{R}_Y\left(\pi/4\right) \cdot \mathbf{R}_X(\omega) \cdot \mathbf{Y}, \tag{45}$$

$$\mathbf{Z}_{2C} = \mathbf{R}_Z(\theta_{C1}) \cdot \mathbf{R}_Y(\alpha) \cdot \mathbf{R}_Z\left(\pi/4\right) \cdot \mathbf{R}_Y(\omega) \cdot \mathbf{Z}. \tag{46}$$

Their developed expressions are:

$$\mathbf{Z}_{2A} = \begin{bmatrix} C\alpha C\omega - C\theta_A S\alpha S\omega \\ \left(1/\sqrt{2}\right)(C\theta_{1A}C\omega S\alpha + C\alpha S\omega - S\theta_{1A}S\alpha) \\ \left(1/\sqrt{2}\right)(C\theta_{1A}C\omega S\alpha + S\theta_{1A}S\alpha + C\alpha S\omega) \end{bmatrix}, \tag{47}$$

$$\mathbf{Z}_{2B} = \begin{bmatrix} \left(1/\sqrt{2}\right)(C\theta_{1B}C\omega S\alpha + S\theta_{1B}S\alpha + C\alpha S\omega) \\ C\alpha C\omega - C\theta_{1B}S\alpha S\omega \\ \left(1/\sqrt{2}\right)((C\theta_{1B}C\omega S\alpha + C\alpha S\omega) - S\theta_{1B}S\alpha) \end{bmatrix}, \tag{48}$$

$$\mathbf{Z}_{2C} = \begin{bmatrix} \left(1/\sqrt{2}\right)((C\theta_{1C}C\omega S\alpha + C\alpha S\omega) - S\theta_{1C}S\alpha) \\ \left(1/\sqrt{2}\right)(C\theta_{1C}C\omega S\alpha + S\theta_{1C}S\alpha + C\alpha S\omega) \\ C\alpha S\omega - C\theta_{1C}S\alpha S\omega \end{bmatrix}. \tag{49}$$

As stated in Eqs. (6) to (8), axes Z_{3k} are written with respect of ψ, θ, and φ which are the SPM end-effector coordinates. By using Euler rotation matrix given by the Eq. (40) we obtain:

$$\mathbf{Z}_{3A} = \begin{bmatrix} -C\theta C\varphi C\psi S\gamma + C\gamma C\psi S\theta + S\gamma S\varphi S\psi \\ C\gamma S\theta S\psi - S\gamma(C\psi S\varphi + C\theta C\varphi S\psi) \\ C\gamma C\theta + C\phi S\gamma S\theta \end{bmatrix}, \tag{50}$$

$$\mathbf{Z}_{3B} = \begin{bmatrix} C\gamma C\psi S\theta - S\gamma\left(S\dfrac{\pi}{3}(C\theta C\psi S\varphi + C\varphi S\psi) + C\dfrac{\pi}{3}(C\theta C\varphi C\psi - S\varphi S\psi)\right) \\ C\gamma S\theta S\psi + S\gamma\left(C\dfrac{\pi}{3}(C\psi S\varphi + C\theta C\varphi S\psi)\right) + S\dfrac{\pi}{3}(C\varphi C\psi - C\theta S\varphi S\psi) \\ C\gamma C\theta - C\left(\dfrac{\pi}{3} + \varphi\right)S\gamma S\theta \end{bmatrix}, \tag{51}$$

$$\mathbf{Z}_{3C} = \begin{bmatrix} C\gamma C\psi S\theta + S\gamma\left(S\dfrac{\pi}{3}(C\theta C\psi S\varphi + C\varphi S\psi) + C\dfrac{\pi}{3}(C\theta C\varphi C\psi - S\varphi S\psi)\right) \\ C\gamma S\theta S\psi + S\gamma\left(C\dfrac{\pi}{3}(C\psi S\varphi + C\theta C\varphi S\psi) - S\dfrac{\pi}{3}(C\varphi C\psi - C\theta S\varphi S\psi)\right) \\ C\gamma C\theta - C\left(\dfrac{\pi}{3}(\pi - 3\varphi)\right)S\varphi S\theta \end{bmatrix}. \tag{52}$$